Experimental research on terahertz Gabor inline digital holography of concealed objects

Qi Li,* Kai Xue, Yun-Da Li, and Qi Wang

National Key Laboratory of Science and Technology on Tunable Laser, Harbin Institute of Technology, P.O. Box 3031, No. 2 YiKuang Street, Harbin 150080, China

*Corresponding author: hit_liqi@yahoo.cn

Received 5 July 2012; revised 30 August 2012; accepted 7 September 2012; posted 10 September 2012 (Doc. ID 171963); published 9 October 2012

Terahertz (THz) radiation has the characteristics of penetrating nonmetallic and nonpolar materials that are opaque to visible light, which makes THz digital holography have an application potential of imaging concealed objects with certain barriers. A CO_2 pumped continuous THz Gabor inline digital holographic imaging system was utilized to conduct experimental researches on imaging concealed objects. Paper, Teflon, a plastic express envelope, and silicon wafers were used as barriers. High-quality reconstructed images were obtained. Compared with the reconstruction results without any barriers, the results verify the feasibility of THz Gabor inline digital holography in imaging concealed objects.

OCIS codes: 110.6795, 090.1995.

1. Introduction

Terahertz (THz) digital holography, which is the combination of THz technology and digital holography, is a frontier science project of THz imaging technology [1–8]. THz digital holography can break through the restriction of diffraction and improve numerical aperture (NA) of the imaging system effectively, which can realize high-quality and high-resolution imaging. Mahon *et al.* have conducted research on 100 GHz millimeter wave off-axis digital holography using the Gunn diode in which a cell detector is used to record holograms in 2006 [1–3]. Heimbeck *et al.* have reported their research results of THz off-axis digital holography in 2011 [4]. The holograms were obtained by means of using a cell detector to scan and the angular spectrum algorithm was used to realize the numerical reconstruction. The systematic resolution is between 1 mm and 1.5 mm. A Russian research group has made a series of experiments on THz Gabor inline digital holography using a tunable THz free electron laser whose working wavelengths were 130 and 68 μm [5,6]. The holograms were recorded by a CCD array detector. Our research group has made a research on 2.52 THz off-axis Fresnel digital holography [8,9]. The pyroelectric camera is used to record holograms and the real lateral resolution is higher than 0.3 mm. The Gabor inline digital holography based on a CO_2 pumped 2.52 THz continuous-wave laser has been realized in 2012 [10]. The pyroelectric camera is used to record holograms and the real lateral resolution can reach 0.2 mm. The required spatial frequency of the detector in inline digital holography is lower than that in off-axis holography, which makes it possible for inline holography to make full use of the limited spatial bandwidth of the detector. Moreover, inline digital holography has the virtues of compact structure and simple setup. The research on inline digital holography is of great significance. Compared with free electron laser, the CO_2 pumped 2.52 THz continuous-wave laser has a lower cost and is easy to operate, which has extensive real applications.

THz imaging has an ability of penetrating nonmetallic and nonpolar barriers to detect concealed objects. It also has an advantage of having lower photon energy, which is safe for the organism. All

1559-128X/12/297052-07$15.00/0

these lead to wide application prospects in some domains like concealed object detecting and security inspection [11–16]. The penetration capability of an imaging system mainly lies on the output power of the THz laser, detector sensitivity and total loss. Compared with the off-axis system, the THz inline digital holography system has the virtues of compact structure, lower energy loss, and higher resolution. THz Gabor inline digital holography for imaging concealed objects is an important application aspect which has not been investigated before. Hence the corresponding experimental research was carried out in this paper for the first time to our knowledge.

2. Imaging Principles

The picture of the experimental setup for recording a Gabor inline hologram is shown in Fig. 1 and the details are shown in [10]. The THz laser is a SIFIR—50 laser, whose operating frequency is 2.52 THz (wavelength of 118.83 μm). The average output power is about 50 mW whose power stability is $< \pm 5\%/\mathrm{h}$. The wave is nearly a Gaussian beam. The pyroelectric camera Pyrocam III is used as the detector whose number of pixels is 124 × 124, and the valid area is 12.4 mm × 12.4 mm. Two off-axis parabolic mirrors (PMs) are used to compose a collimated lens combination. A reflecting mirror is adopted to change the beam direction to make it convenient for recording. BS1 is a high-resistivity monocrystal silicon wafer whose transmissivity is nearly 99% for 2.52 THz. When the collimated wave illuminates the object, the wave modulated by the object information is used as object wave, and the rest transmitting wave is reference wave. The object wave and reference wave interfere in the detector surface to form the interference pattern.

There is a restriction in Gabor inline digital holography where the transparent area of the recorded object must be larger than the opaque area. The field distribution in the object plane after plane wave illuminating the object plane x_0-y_0 vertically can be expressed as follows:

$$U(x_0, y_0) = 1 - a(x_0, y_0), \tag{1}$$

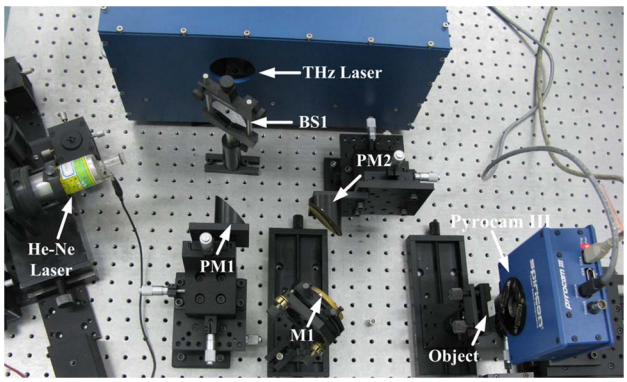

Fig. 1. (Color online) Picture of the experimental setup for recording a Gabor inline hologram.

where the left term $U(x_0, y_0)$ is the whole complex amplitude distribution in the object plane and the term $a(x_0, y_0)$ is the contribution of the opaque area, which both reflect the object information. The equation is considered as the superimposition of the reference wave and object wave.

The complex amplitude distribution in the hologram plane x-y based on Rayleigh–Sommerfeld diffraction integral function and the corresponding approximation can be approximately expressed as follows [10,17]:

$$\tilde{I}(x, y) \approx 1 - a(x_0, y_0) * h_z(x_0, y_0, z) - a^*(x_0, y_0) * h_z^*(x_0, y_0, z), \tag{2}$$

where $h_z(x_0, y_0, z)$ represents the impulse response function, $*$ is convolution operation, the superscript $*$ represents complex conjugate, and z is the recording distance between the object plane and hologram plane. The first term in Eq. (2) is the DC term, which has little effect on the reconstructed image.

Assume that the image plane $x_I - y_I$ is z away from the hologram plane. As the plane wave, whose amplitude is 1, is utilized for numerical reconstruction, the complex amplitude distribution in the image plane is as follows [10]:

$$U(x_I, y_I) = U(x_0, y_0) - a^*(x_0, y_0) * h_{2z}^*(x_0, y_0, z). \tag{3}$$

Equation (3) can be solved by a convolution reconstruction algorithm and then the object distribution is obtained. The applicable condition of a convolution reconstruction algorithm is as follows:

$$\frac{|z|}{X} \geq \left(\frac{|z|}{X}\right)_{\max} = \begin{cases} \sqrt{\frac{1}{(\lambda/\Delta x)^2} - \frac{1}{4}\left[\left(\frac{Y}{X}\right)^2 + 1\right]} & \text{if } \frac{Y}{X}\frac{\Delta y}{\Delta x} \leq 1 \\ \sqrt{\frac{(Y/X)^2(\Delta y/\Delta x)^2}{(\lambda/\Delta x)^2} - \frac{1}{4}\left[\left(\frac{Y}{X}\right)^2 + 1\right]} & \text{if } \frac{Y}{X}\frac{\Delta y}{\Delta x} \geq 1 \end{cases}, \tag{4}$$

where the spacing of the sampling point is $\Delta x \times \Delta y$ in the object plane, the sampling number is $N \times M$, and the sampling area $X \times Y$ is $X \times Y = N\Delta x \times M\Delta y$.

The barriers used in the experiments are paper, Teflon, a polyethylene plastic express envelope, and high-resistivity monocrystal silicon wafers whose transmissivities are 0.368, 0.842, 0.903, and 0.988, respectively.

The field distributions after the collimated wave penetrating the barriers are shown in Fig. 2. It is obvious that there are great differences in the field distributions because of different materials and different material distributions. The attenuation of papers is the worst, and the transmitting light intensity has serious aberration, which is mainly caused by nonuniform materials. The field distribution

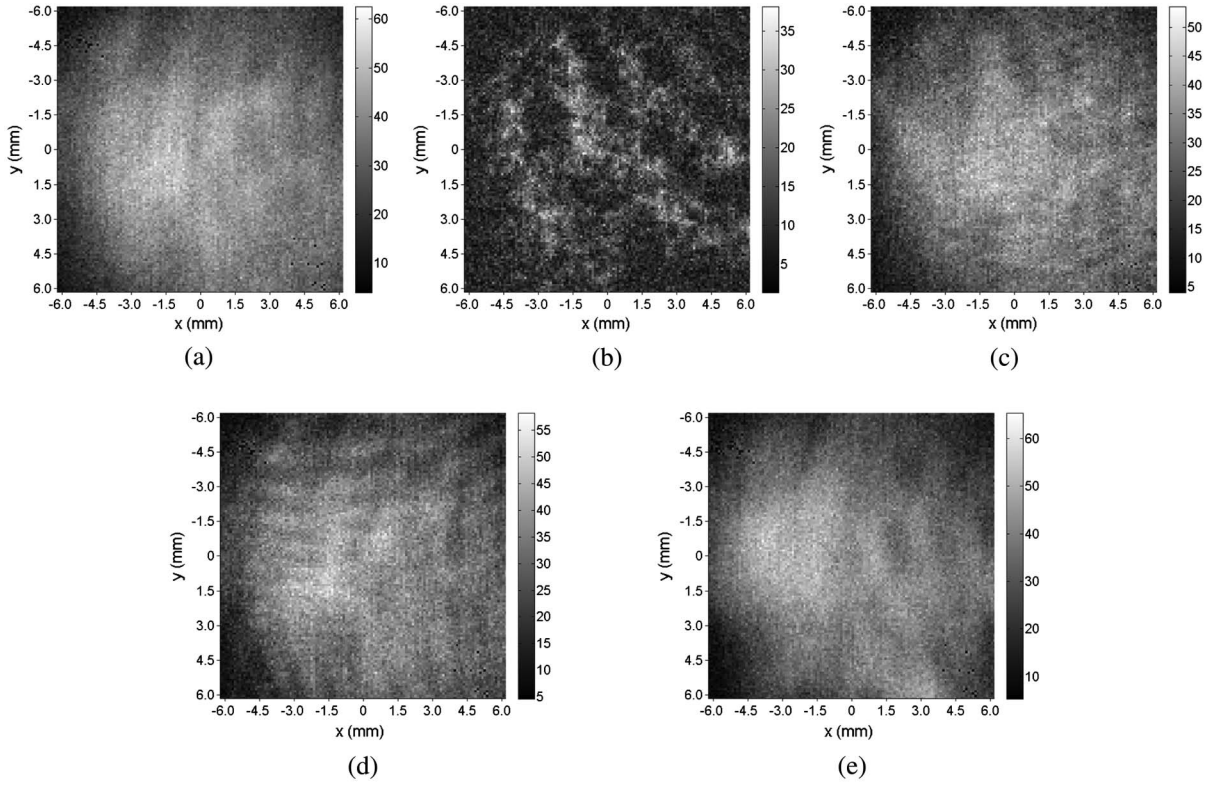

Fig. 2. Illumination light field distribution and field distributions penetrating barriers: (a) illumination light field distribution (b) paper, (c) Teflon, (d) plastic express envelope, and (e) silicon wafer.

penetrating a plastic express envelope has slight stripes, which is caused by the creases; however, the effect on the whole field distribution is small. The field distributions penetrating Teflon and silicon wafers preserve illumination light field distribution well.

3. Results and Analysis

Firstly, 0.3 mm resolution charts are used as the imaging objects. In order to restrain the effect of random noise on the holograms and reconstruction results, the holograms of the resolution charts are all 40-frame averaging results.

When the recording distance is $z = 25$ mm, the ideal lateral resolution is about 0.238 mm. However, aperture integral effect, detector sensitivity, and system energy loss will result in real lateral resolution less than the ideal resolution. Therefore a 0.3 mm lateral stripe resolution chart is chosen as the imaging object, which is shown in Fig. 3. The object is placed in front of the photosensitive surface and the recording distance is about 24 mm. The reconstructed image of the 0.3 mm object, without any barriers is shown in Fig. 4. The object position is fixed and the barriers are inserted in front of the object, alternately. The holograms with different barriers are recorded and the Rayleigh–Sommerfeld convolution algorithm is utilized to conduct numerical reconstruction.

The reconstruction results of lateral stripes, with different barriers are shown in Fig. 5. It can be found that the THz inline digital holographic system can still realize image reconstruction of concealed objects after penetrating the barriers. Compared with the

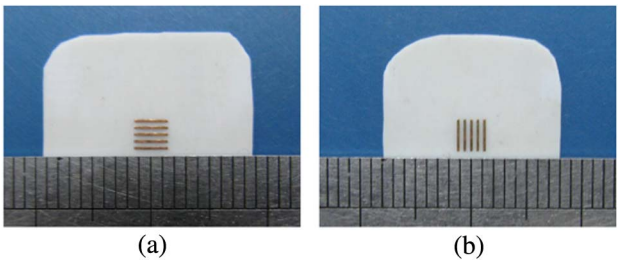

Fig. 3. (Color online) 0.3 mm resolution chart object: (a) lateral stripes object and (b) longitudinal stripes object.

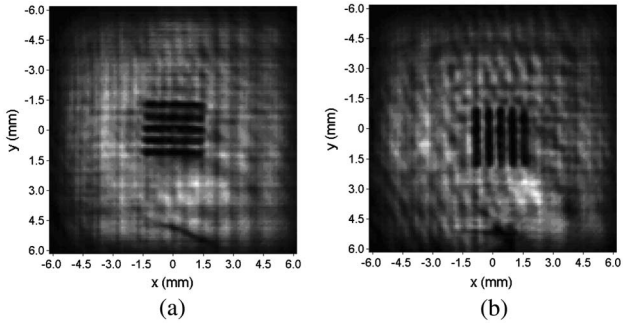

Fig. 4. Reconstruction result of the 0.3 mm resolution chart object without barriers: (a) lateral stripes object and (b) longitudinal stripes object.

result in Fig. 4, although the image quality of the reconstructed images after penetrating the Teflon, a plastic express envelope, and the silicon wafer declines slightly, the reconstructed images are still distinct, have a high contrast, and have prominent edge details. Meanwhile, it can be inferred that the reconstructed stripes widen appreciably, and there are many blocked light spots in the reconstructed background. These are mainly because the inserted barriers change the light field distribution, which leads to an aberration in the transmitting light field. These distortions affect the reconstructed image quality greatly.

Furthermore, compare the result by inserting a paper with the other reconstruction results in Fig. 5 and we can find that the reconstructed image quality declines, the object edge blurs, and the whole contrast decreases, obviously. However, the contour is still distinguishable except that some details are lost. The paper has a severe attenuation on 2.52 THz

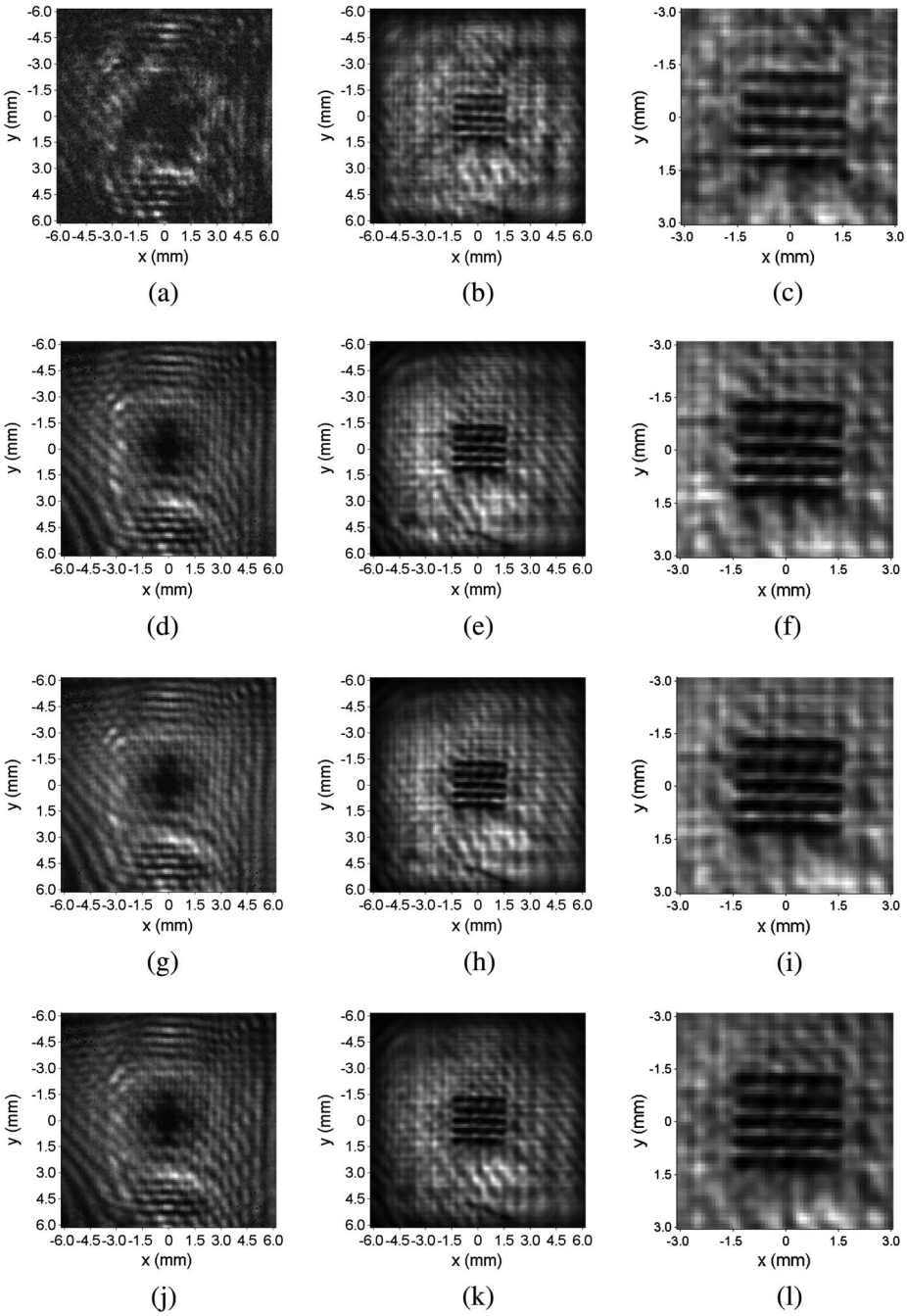

Fig. 5. Reconstruction results of 0.3 mm lateral stripes after penetrating different barriers: (a) hologram after penetrating a paper, (b) reconstructed image of (a), (c) enlarged image of (b), (d) hologram after penetrating Teflon, (e) reconstructed image of (d), (f) enlarged image of (e), (g) hologram after penetrating a plastic express envelope, (h) reconstructed image of (g), (i) enlarged image of (h), (k) hologram after penetrating a silicon wafer, (j) reconstructed image of (k), (l) enlarged image of (j).

radiation, which makes the light energy decline. This results in the interference fringe intensity recorded in the hologram plane dropping greatly. The detector sensitivity is relatively low, which leads to the loss of some useful interference information. All this makes it impossible to reveal the details in the reconstructed image. Meanwhile, the nonuniform material distribution of the paper also causes a distortion in the transmitting light field, which will also depress the image quality.

In the meantime, a 0.3 mm longitudinal stripe chart is also used as the imaging object. The recording distance is still about 24 mm and the same experiments are conducted. The reconstruction results are shown in Fig. 6.

It can be inferred in Figs. 5 and 6 that the contrast of the reconstruction of the longitudinal stripes is better than that of the lateral stripes. The possible reasons are as follows. On the one hand, the lateral distribution of the collimated wave is larger than the

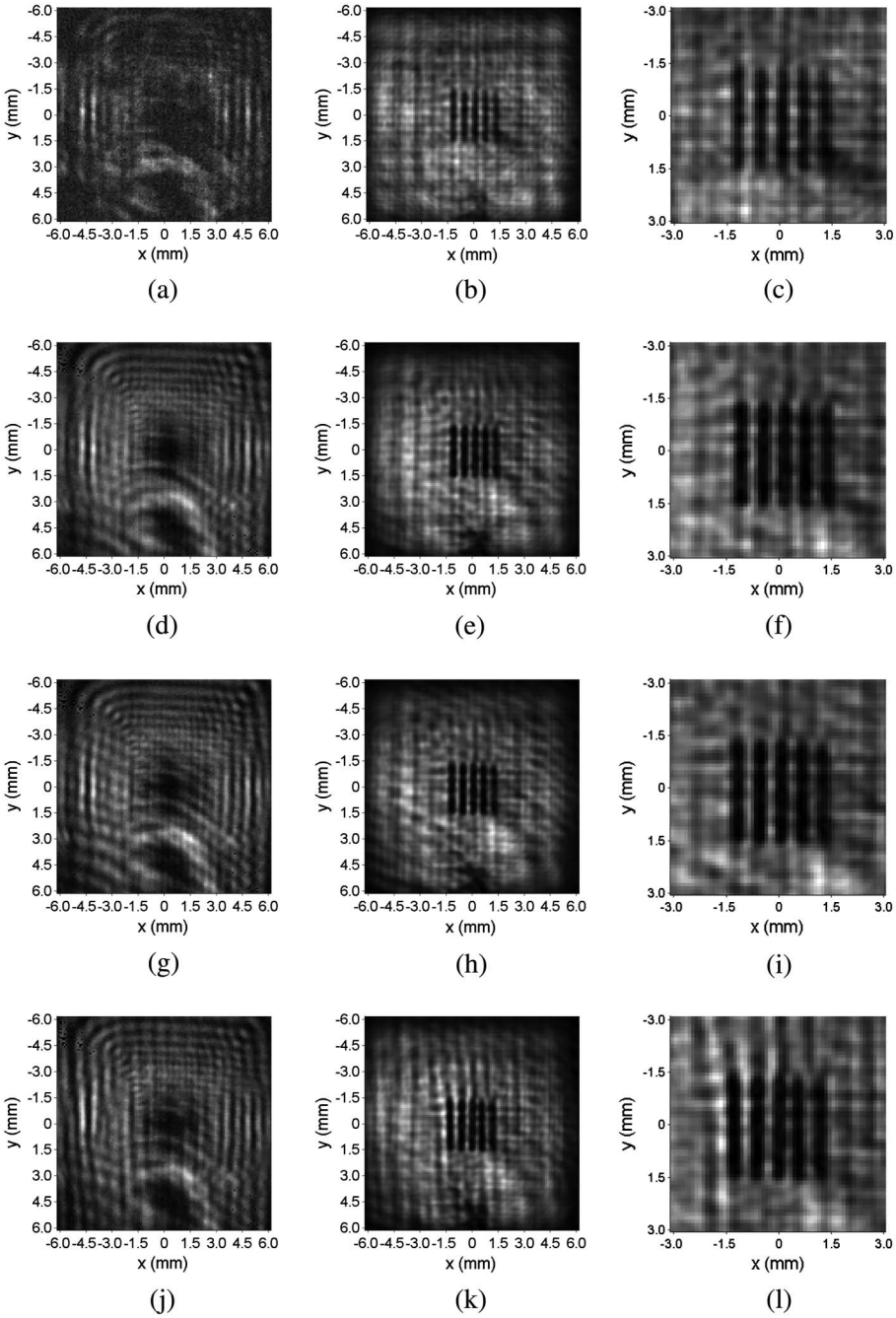

Fig. 6. Reconstruction results of 0.3 mm longitudinal stripes after penetrating different barriers: (a) hologram after penetrating a paper, (b) reconstructed image of (a), (c) enlarged image of (b), (d) hologram after penetrating Teflon, (e) reconstructed image of (d), (f) enlarged image of (e), (g) hologram after penetrating a plastic express envelope, (h) reconstructed image of (g), (i) enlarged image of (h), (k) hologram after penetrating a silicon wafer, (j) reconstructed image of (k), (l) enlarged image of (j).

Fig. 7. (Color online) Picture of a sheet metal object.

longitudinal distribution which is shown in Fig. 2(a). The energy mainly focuses on the lateral center area. The detector sensitivity is finite. The interference information of the longitudinal stripes concentrates on the center domains of the left and right side of the hologram, and the interference information of the lateral stripes concentrates on the center domains of the upper and lower side of the hologram. The interference information of the longitudinal stripes is relatively easier to be recorded. On the other hand, the output power of the laser in the longitudinal stripe imaging experiments is appreciably higher than that in the lateral stripe imaging experiments, and the former is 1.2 times the latter, which could improve the reconstructed image contrast. The imaging characteristic of the longitudinal stripes is nearly the same as that of the lateral stripes and hence the detailed analysis is omitted.

Then a sheet metal object, which is common in daily life, is used as the imaging object. The object is pasted up on a piece of cellulose tape. The diameter of the sheet metal is about 4 mm and the picture is shown in Fig. 7. The cellulose tape is placed facing the detector. Firstly, a paper is used as the barrier. The sheet metal is nearly 45 mm away from the photosurface, and the distance between the paper and sheet metal is about 90 mm. The holograms and corresponding reconstructed images (with and without a barrier) are shown in Fig. 8. The numbers of frames are 1 and 20, respectively. It is found that the sheet metal can be reconstructed relatively clear with a single-frame hologram. When the object is blocked partially, the blocked area of the reconstructed image is dim, and the image quality of the transparent area declined. After being blocked completely by the paper, the reconstruction result is fuzzy and the image quality descends greatly. The possible reasons are as follows. As has been

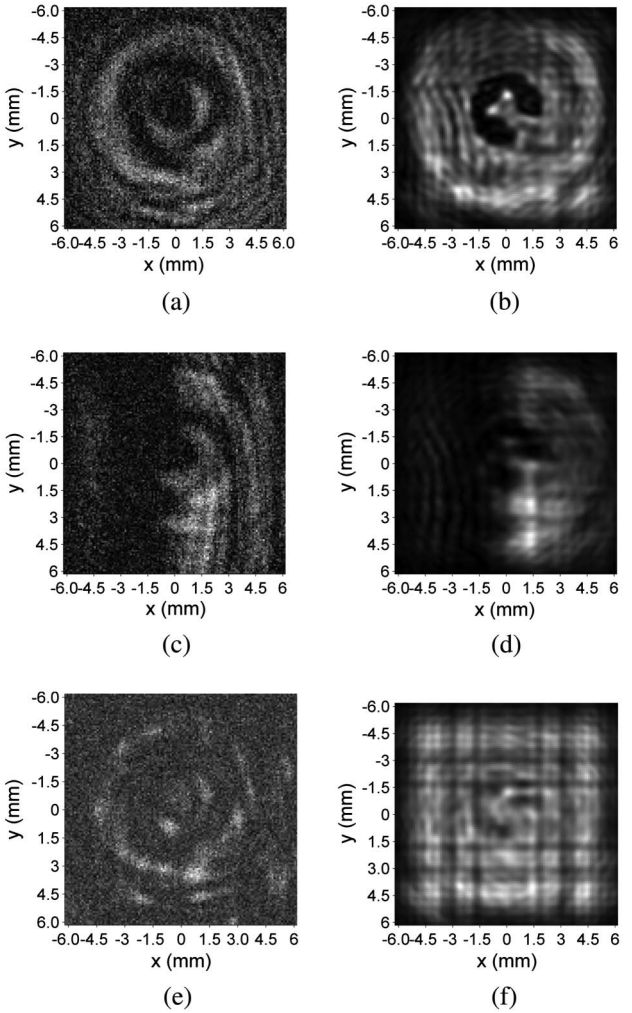

Fig. 8. Reconstruction results of the sheet metal object after penetrating a paper: (a) single-frame hologram without a barrier, (b) reconstructed image of (a), (c) single-frame hologram after being blocked partially by a paper, (d) reconstructed image of (c), (e) 20-frame hologram after being blocked completely by a paper, and (f) reconstructed image of (e).

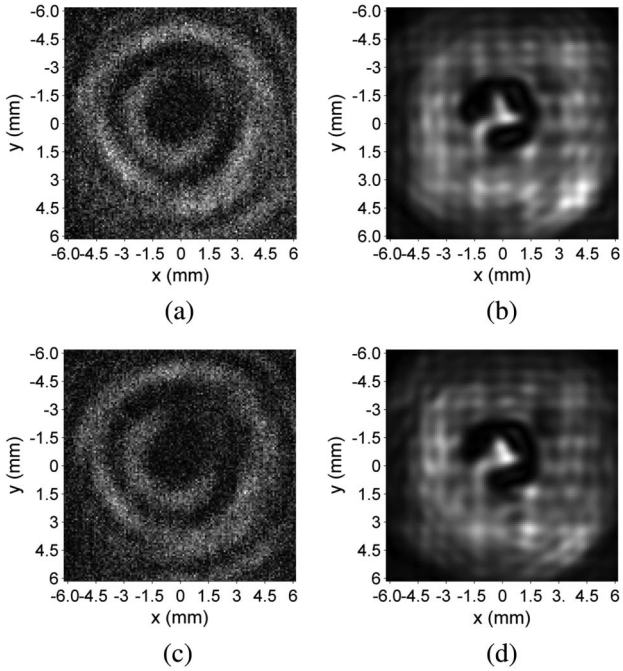

Fig. 9. Reconstruction results of the sheet metal object after penetrating a polyethylene express envelope: (a) single-frame hologram without a barrier, (b) reconstructed image of (a), (c) single-frame hologram after being blocked completely by a polyethylene express envelope, and (d) reconstructed image of (c).

mentioned above, Gabor inline digital holography has a restriction that the transparent area of the recorded object must be larger than the opaque area, and the insert of a paper has an impact on the transparent area. Furthermore, the granules on the transparent area result in coherent light being partially incoherent, which would debase the reconstruction quality. The superposition effect of these two reasons makes the reconstructed images with a barrier of a paper fuzzy. However, the contour is still approximately distinguishable.

Finally, a polyethylene plastic express envelope is used as the barrier. The sheet metal is nearly 71 mm away from the photosurface, and the distance between the paper and sheet metal is about 35 mm. The cellulose tape is placed opposite to the detector. The holograms and corresponding reconstructed images, with and without a polyethylene plastic express envelope, are shown in Fig. 9. The numbers of frames are all 1. It can be inferred that the reconstructed images are all relatively clear compared to those with paper. The possible reason is that the transmissivity of polyethylene is better than that of paper in the THz domain, which can relatively satisfy the restriction condition of Gabor inline digital holography better.

4. Conclusion

THz imaging technology has the capability of imaging concealed objects because of the unique characteristics of THz radiation. To take full advantage of the THz imaging technology, experimental research has been conducted with THz inline digital holographic imaging on concealed objects. For the first time experiments have been conducted using paper, Teflon, a polyethylene plastic express envelope, and silicon wafers. High-quality reconstruction results are obtained by imaging the 0.3 mm resolution chart and a sheet metal object. The results verify the feasibility of THz Gabor inline digital holography in imaging concealed objects, which has great application potentials.

This work was supported by the Specialized Research Fund for the Doctoral Program of Higher Education (SRFDP) of China 20112302110028.

References

1. R. J. Mahon, J. A. Murphy, and W. Lanigan, "Digital holography at millimetre wavelengths," Opt. Commun. **260**, 469–473 (2006).
2. R. J. Mahon, J. A. Murphy, and W. Lanigan, "Terahertz holographic image reconstruction and analysis," in *2004 Joint 29th International Conference on Infrared and Millimeter Waves* (IEEE, 2004), pp. 749–750.
3. I. McAuley, J. A. Murphy, N. Trappe, R. Mahon, D. McCarthy, and P. McLaughlin, "Applications of holography in the millimeter-wave and terahertz region," Proc. SPIE **7939**, 79380H (2011).
4. M. S. Heimbeck, M. K. Kim, D. A. Gregory, and H. O. Everitt, "Terahertz digital holography using angular spectrum and dual wavelength reconstruction methods," Opt. Express **19**, 9192–9200 (2011).
5. V. S. Cherkassky, B. A. Knyazev, S. V. Kozlov, V. V. Kubarev, G. N. Kulipanov, A. N. Matveenko, V. M. Popik, D. N. Root, P. D. Rudych, O. A. Shevchenko, A. V. Trifutina, and N. A. Vinokurov, "Terahertz imaging and holography with a high-power free electron laser," in *2005 Joint 30th International Conference on Infrared and Millimeter Waves & 13th International Conference on Terahertz Electronics*, Vol. **2** (IEEE, 2005), pp. 337–338.
6. B. A. Knyazev, A. L. Balandin, V. S. Cherkassky, Y. Y. Choporova, V. V. Gerasimov, M. A. Demyanenko, D. G. Esaev, A. A. Nikitin, V. V. Pickalov, M. G. Vlasenko, D. G. Rodionov, and O. A. Shevchenko, "Classic holography, tomography and speckle metrology using a high-power terahertz free electron laser and real-time image detectors," in *2010 International Conference on Infrared, Millimeter, and Terahertz Waves* (IEEE, 2010), pp. 1–3.
7. Y. Zhang, W. Zhou, X. Wang, Y. Cui, and W. Sun, "Terahertz digital holography," Strain **44**, 380–385 (2008).
8. S.-H. Ding, Q. Li, Y.-D. Li, and Q. Wang, "Continuous-wave terahertz digital holography by use of a pyroelectric array camera," Opt. Lett. **36**, 1993–1995 (2011).
9. Q. Li, S. H. Ding, Y. D. Li, and Q. Wang, "Experimental research on resolution improvement in cw THz digital holography," Appl. Phys. B **107**, 103–110 (2012).
10. K. Xue, Q. Li, Y.-D. Li, and Q. Wang, "Continuous-wave terahertz inline digital holography," Opt. Lett. **37**, 3228–3230 (2012).
11. A. R. Sanchez and X.-C. Zhang, "Terahertz science and technology trends," IEEE J. Sel. Top. Quantum Electron. **14**, 260–269 (2008).
12. K. Kawase, Y. Ogawa, Y. Watanabe, and H. Inoue, "Non-destructive terahertz imaging of illicit drugs using spectral fingerprints," Opt. Express **11**, 2549–2554 (2003).
13. A. W. M. Lee and Q. Hu, "Real-time, continuous-wave terahertz imaging by use of a microbolometer focal-plane array," Opt. Lett. **30**, 2563–2565 (2005).
14. A. W. M. Lee, B. S. Williams, and S. Kumar, "Real-time imaging using a 4.3 THz quantum cascade laser and a 320 × 240 microbolometer focal-plane array," IEEE Photon. Technol. Lett. **18**, 1415–1417 (2006).
15. B. N. Behnken and G. Karunasiri, "Real-time terahertz imaging of nonmetallic objects for security screening and anti-counterfeiting applications," Proc. SPIE **7117**, 711705 (2008).
16. N. Karpowicz, H. Zhong, C. Zhang, K.-I. Lin, J.-S. Hwang, J. Xu, and X.-C. Zhang, "Compact continuous-wave subterahertz system for inspection applications," Appl. Phys. Lett. **86**, 054105 (2005).
17. L. Denis, C. Fournier, T. Fournel, and C. Ducottet, "Twin-image noise reduction by phase retrieval in inline digital holography," Proc. SPIE **5914**, 59140J (2005).